Inverse scattering designs of dispersion-engineered planar waveguides

Alexander R. May,* Francesco Poletti, and Michalis N. Zervas

Optoelectronics Research Centre, University of Southampton, Southampton, SO17 1BJ, UK
*arm103@orc.soton.ac.uk

Abstract: We have introduced a semi-analytical IS technique suitable for multipole, rational function reflection coefficients, and used it for the design of dispersion-engineered planar waveguides. The technique is used to derive extensive dispersion maps, including higher dispersion coefficients, corresponding to three-, five- and seven-pole reflection coefficients. It is shown that common features of dispersion-engineered waveguides such as refractive-index trenches, rings and oscillations come naturally from this approach when the magnitude of leaky poles in increased. Increasing the number of poles is shown to offer a small but measureable change in higher order dispersion with designs dominated by a three pole design with a leaky pole pair of the smallest modulus.

OCIS codes: (060.2280) Fiber design and fabrication; (290.3200) Inverse scattering.

References and links

1. S. Ramachandran, "Dispersion-tailored few-mode fibers : a versatile platform for in-fiber photonic devices," J. Lightwave Technol. **23**(11), 3426–3443 (2005).
2. M. Wandel and P. Kristensen, "Fiber designs for high figure of merit and high slope dispersion compensating fibers," J. Opt. Fiber Commun. **3**(1), 25–60 (2006).
3. G. P. Agrawal, *Nonlinear Fiber Optics* (Academic, 2001).
4. J. M. Dudley and S. Coen, "Supercontinuum generation in photonic crystal fiber," Rev. Mod. Phys. **78**(4), 1135–1184 (2006).
5. M. Takahashi, R. Sugizaki, J. Hiroishi, M. Tadakuma, Y. Taniguchi, and T. Yagi, "Low-loss and low-dispersion-slope highly nonlinear fibers," J. Lightwave Technol. **23**(11), 3615–3624 (2005).
6. M. Onishi, T. Okuno, T. Kashiwada, S. Ishikawa, N. Akasaka, and M. Nishimura, "Highly nonlinear dispersion-shifted fibers and their application to broadband wavelength converter," Opt. Fiber Technol. **4**(2), 204–214 (1998).
7. L. Gruner-Nielsen, M. Wandel, P. Kristensen, C. Jorgensen, L. V. Jorgensen, B. Edvold, B. Palsdottir, and D. Jakobsen, "Dispersion-compensating fibers," J. Lightwave Technol. **23**(11), 3566–3579 (2005).
8. R. Feced, M. N. Zervas, and M. A. Muriel, "An efficient inverse scattering algorithm for the design of nonuniform fiber Bragg gratings," J. Quantum Electron. **35**(8), 1105–1115 (1999).
9. J. Skaar, L. Wang, and T. Erdogan, "On the synthesis of fiber Bragg gratings by layer peeling," J. Quantum Electron. **37**(2), 165–173 (2001).
10. M. Ibsen, M. K. Durkin, M. N. Zervas, A. B. Grudinin, and R. I. Laming, "Custom design of long chirped Bragg gratings: application to gain-flattening filter with incorporated dispersion compensation," IEEE Photon. Technol. Lett. **12**(5), 498–500 (2000).
11. M. N. Zervas and M. K. Durkin, "Physical insights into inverse-scattering profiles and symmetric dispersionless FBG designs," Opt. Express **21**(15), 17472–17483 (2013).
12. S. Lakshmanasamy and A. K. Jordan, "Design of wide-core planar waveguides by an inverse scattering method," Opt. Lett. **14**(8), 411–413 (1989).
13. A. K. Jordan and S. Lakshmanasamy, "Inverse scattering theory applied to the design of single-mode planar optical waveguides," J. Opt. Soc. Am. A **6**(8), 1206–1212 (1989).
14. C. Papachristos and P. Frangos, "Synthesis of single-and multi-mode planar optical waveguides by a direct numerical solution of the Gel'fand-Levitan-Marchenko integral equation," Opt. Commun. **203**(1-2), 27–37 (2002).
15. I. Hirsh, M. Horowitz, and A. Rosenthal, "Design of planar waveguides with prescribed mode-profile using inverse scattering theory," J. Quantum Electron. **45**(9), 1133–1141 (2009).
16. M. Cvijetic, "Dual-mode optical fibres with zero intermodal dispersion," Opt. Quantum Electron. **16**(4), 307–317 (1984).

#223305 - $15.00 USD Received 16 Sep 2014; revised 24 Dec 2014; accepted 18 Jan 2015; published 3 Feb 2015

17. A. K. Jordan and S. Ahn, "Inverse scattering theory and profile reconstruction," Proc. Inst. Electr. Eng. **126**(10), 945–950 (1979).
18. S. Ahn and A. K. Jordan, "Profile inversion of simple plasmas and nonuniform regions: three-pole reflection coefficient," IEEE Trans. Antenn. Propag. **24**(6), 879–882 (1976).
19. M. Reilly and A. K. Jordan, "The applicability of an inverse method for reconstruction of electron-density profiles," IEEE Trans. Antenn. Propag. **29**(2), 245–252 (1981).
20. I. Kay, "The inverse scattering problem when the reflection coefficient is a rational function," Commun. Pure Appl. Math. **13**(3), 371–393 (1960).
21. J. Xia, A. K. Jordan, and J. A. Kong, "Inverse-scattering view of modal structures in inhomogeneous optical waveguides," J. Opt. Soc. Am. A **9**(5), 740–748 (1992).
22. P. Deift and E. Trubowitz, "Inverse scattering on the line," Commun. Pure Appl. Math. **32**(2), 121–251 (1979).
23. K. R. Pechenick and J. M. Cohen, "Inverse scattering—exact solution of the Gel'fand-Levitan equation," J. Math. Phys. **22**(7), 1513–1516 (1981).
24. D. B. Ge, A. K. Jordan, and L. S. Tamil, "Numerical inverse scattering theory for the design of planar optical waveguides," J. Opt. Soc. Am. A **11**(11), 2809 (1994).
25. K. R. Pechenick and J. M. Cohen, "Exact solutions to the valley problem in inverse scattering," J. Math. Phys. **24**(2), 406–409 (1983).
26. A. Akritas and P. Vigklas, "Counting the number of real roots in an interval with Vincent's theorem," Bull. Math. Soc. Sci. Math. Roum. **53**, 201–211 (2010).
27. K. Case, "On wave propagation in inhomogeneous media," J. Math. Phys. **13**(3), 360 (1972).
28. Maplesoft, "MAPLE," (2012).

1. Introduction

Optical waveguides, in addition to controlling the propagation losses through total internal reflections and efficient power confinement in the core, offer the unique ability to control the group velocity of the propagating light. These two main attributes have rendered optical waveguides indispensable parts in any advanced optical system. So far, the largest control and highest performance has been achieved with optical fibers. Tailoring the core shape has been used to control both modality and group velocity dispersion in optical fibers [1].

While the control of dispersion in optical fibers is usually associated with dispersion compensation in optical communications networks [2] there has also being increasing interest in its control for the purposes of harnessing and optimizing nonlinear optical effects. Parametric processes [3] and supercontinuum generation [4] rely upon tailoring the dispersion profile of the fiber to enhance energy transfer in certain spectral regions. Therefore, significant effort has been put over the last decade to develop technologies to fine control waveguide dispersion [5].

Silica-based highly nonlinear fibers (HNLF) feature very low attenuation characteristics and so by using long lengths of these fibers a large nonlinear effect can be realized. Small mode effective areas and thereby large nonlinearity are produced by increasing the refractive index (RI) difference between the core and the cladding which enhances the confinement of the light. This may be achieved by utilizing a highly germanium-doped core and a fluorine-doped cladding. In addition to creating a small mode effective area, nonlinear processes such as four-wave mixing (FWM) require the pump wavelength to coincide with the zero-dispersion wavelength of the fiber. Further control of the dispersion slope is advantageous in controlling dispersion and increasing operating bandwidth. An example of a HNLF with a zero-dispersion wavelength near 1550nm, a mode field diameter (MFD) of 4.3μm and a low dispersion slope of 0.0032ps/nm^2/km was realized through the use of a W-shape RI profile [6]. The index and thickness of these RI features determines the rate as a function of wavelength at which the mode transitions from the core to the ring. It is this, as well as, the average RI over which the mode extends that controls the propagation constant and its derivatives and thereby the dispersion properties of the fiber.

Control of dispersion has been achieved by modifying the inner-core shape and adding features, such as rings and trenches into the overall core design [1,7]. While the dispersion-engineering of fibers is typically approached through a trial and error method and parametric study, a powerful method for designing dispersion-engineered devices is *inverse scattering* (IS). Such methods have been used extensively to design fiber Bragg gratings with prescribed dispersion characteristics [8–10]. These methods have provided non-intuitive designs with advanced performance [11].

Also authors have in the past studied the design of planar waveguides, as well as, fibers from the IS point of view [12–17]. In these works, the modal properties of the waveguide such as a prescribed mode-profile [15], or the number of propagating modes [14] has been considered and specified at the start and through the inverse design process the waveguide with these properties is obtained. In particular, in the latter work the starting point of a truncated reflectionless potential was used. However, in each case, waveguide dispersion has not been considered from the point of view of the selection of (a variable number of) leaky poles and their approximation to the associated radiation modes. In our work, a transverse reflection coefficient of the structure is defined and the guiding properties of the waveguides are defined by the positions of reflection coefficient poles on the complex plane, representing guided and leaky modes of the waveguide under consideration. Similar IS techniques have also been used for the determination of the ionosphere characteristics from reflection data [18,19].

In this paper, we extend IS techniques, used in the ionosphere characterization, for the design of optical planar waveguides and study their dispersion characteristics. To our knowledge this is the first time that the connection between a transverse reflection coefficient and waveguide dispersion has been investigated. New designs are obtained with RI features which are generalizations to the ones considered previously. As a starting point to a more general analysis with fibers, we describe the dispersion characteristics of IS designed planar waveguides. We begin with an overview of IS theory before considering design cases for which exact solutions exist which have previously been discussed in the literature, before extending this to a set of new cases. We then show that typical dispersion-engineered waveguide features such as rings and trenches come naturally from this theory. We finally discuss what benefits the new extended cases bring to the literature.

2. Inverse Scattering Theory

If we consider a planar optical waveguide with a varying RI *n(x)* surrounded by two cladding layers of constant index n_2 as shown in Fig. 1, the supported TE modes are of the form:

$$E_y(x,z,t) = E_{y0}(x,k_0)\exp(i\beta z)\exp(-i\omega t) \tag{1}$$

where z is the direction of propagation, ω is the angular frequency, β is the propagation constant along the z-axis and k_0 is the free-space wave number. In this case, the vector wave equations reduce to:

$$\frac{d^2E_y}{dx^2} + \left[k_0^2 n(x)^2 - \beta^2\right]E_y = 0 \tag{2}$$

which can be rewritten as a Schrodinger equations:

$$\frac{d^2E_y}{dx^2} + \left[k^2 - q(x)\right]E_y = 0 \tag{3}$$

where

$$k^2 = k_0^2 n_2^2 - \beta^2 \tag{4}$$

is the transverse propagation constant and the potential $q(x)$ is of the form:

$$q(x) = k_0^2\left[n_2^2 - n(x)^2\right] \tag{5}$$

The waveguide can also be considered as a general scatterer, which under plane-wave normal incidence gives a reflection coefficient $r(k)$ (see Fig. 1). The RI profile $n(x)$ of the optical waveguide can then be determined from its transverse reflection coefficient $r(k)$ through the solution of the Gel'fand-Levitan-Marchenko (GLM) integral equation [20] for the unknown kernel $K(x,t)$ [13]:

$$R(x+t)+K(x,t)+\int_{-t}^{x} K(x,y)R(x+y)dy=0 \tag{6}$$

where $x \geq |t|$, and the reflected transient $R(t)$ is given as [13]:

$$R(t)=\frac{1}{2\pi}\int_{-\infty}^{\infty} r(k)\exp(-ikt)dk - i\sum_{p=1}^{n} r_p \exp(-ik_p t) \tag{7}$$

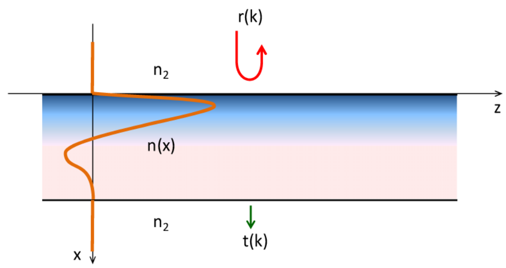

Fig. 1. The physical model for electromagnetic reflection from an inhomogeneous planar waveguide.

The transverse reflection coefficient is obtained by considering a plane wave of propagation constant k impinging on the planar waveguide at normal incidence. In the GLM formulation, the reflection coefficient $r(k)$ is considered to be a rational function, of which poles k_p on the positive imaginary axis correspond to guided modes with corresponding residues r_p. Complex poles, on the other hand, correspond to leaky modes. In this case, the integral in Eq. (7) corresponds to the continuous spectrum of radiation modes, while the sum to the discrete set of guided modes [14,21]. The kernel $K(x,t)$ can be obtained by solving Eq. (6), and the potential is then derived from the relation [13]:

$$q(x)=2\frac{dK(x,x)}{dx} \tag{8}$$

Finally, the refractive index profile is obtained from:

$$n(x)=\sqrt{n_2^{\,2}-\frac{q(x)}{k_0^{\,2}}} \tag{9}$$

The profile is defined at the wavelength of interest λ_0 through $k_0 = 2\pi/\lambda_0$.

A general reflection coefficient can be approximated by rational functions of different degree [19]. The three-pole case is amenable to analytic solutions and has been studied extensively in the past in the context of ionospheric simulations [17] and waveguide modality [12,13]. So far, waveguide examples are based upon either the GLM procedure or the application of the Crum-Krein or Darboux transformations [22] to reflectionless potentials. Here we focus on the GLM technique where we note that to date the majority of waveguide examples are based upon a rational three-pole formulation. While numerical GLM techniques exist for non-rational reflection coefficients, these methods bring with it the possibility of roundoff errors and instabilities [23] and there is therefore an advantage in solving the GLM

#223305 - $15.00 USD Received 16 Sep 2014; revised 24 Dec 2014; accepted 18 Jan 2015; published 3 Feb 2015

equation exactly using a generalization of the seminal work of Kay [20]. In addition, the complexity of the solutions, however, increases quickly with the number of poles and in view of Galois' proof that 5th and higher-order polynomial equations are insoluble by radicals, the previous analytic solutions cannot be implemented. In this case, the semi-analytical numerical technique, described by Pechenick in the context of ionospheric reflection data inversion [23], provides a powerful alternative. We have used this general technique throughout our study. It is worth noting that this is, to our knowledge, the first time this technique has been applied to waveguiding structures and the lack of significant development of the inversion of potentials with bound states is acknowledged in the work of Ge et al. [24].

3. Designs using rational reflection coefficients

We begin our study by considering first the simplest case of three-pole reflection coefficients and then proceed by progressively increasing the number of poles to five and seven.

3.1 Three-pole reflection coefficients

First we consider waveguide designs associated with the three-pole reflection coefficients:

$$r(k)=\frac{k_1k_2k_3}{(k-k_1)(k-k_2)(k-k_3)} \tag{10}$$

with poles k_1, k_2 and k_3 given by:

$$k_1=-c_1-ic_2;\quad k_2=c_1-ic_2;\quad k_3=+ia \tag{11}$$

for which $c_1, c_2, a\in R^+$. The choice of poles k_1, k_2 and k_3 controls the shape and dispersion of reflection coefficient of the scattering layered medium and is expected to define the dispersion of the resulting waveguide. Pole k_3 corresponds to the propagation constant of the fundamental guided mode through $\beta=\sqrt{k_0^2n_2^2+a^2}$. Poles k_1 and k_2 on the other hand, result in leaky modes, which are necessary for the full description of the waveguide. Poles k_1 and k_2 are hereafter referred to as "leaky poles".

In order for a solution to exist, the reflection coefficient must obey a set of conditions [25], which are indeed satisfied by the general forms given in Eq. (11). However, it is necessary to restrict the position of the poles in the complex plane in order to satisfy energy conservation, $r(k)\leq 1$, for all real k. Previous authors [12,13] have satisfied this requirement by considering the discriminant of a conservation-of-energy condition to be positive, thus giving the allowed regions A and B shown in Fig. 2. Region A is bounded above by the line $c_2 = 0.5$ and below by the lemniscate of Bernoulli [25]. Region B is bounded below by $c_2 = 0.5$, but it is unbounded above.

#223305 - \$15.00 USD Received 16 Sep 2014; revised 24 Dec 2014; accepted 18 Jan 2015; published 3 Feb 2015

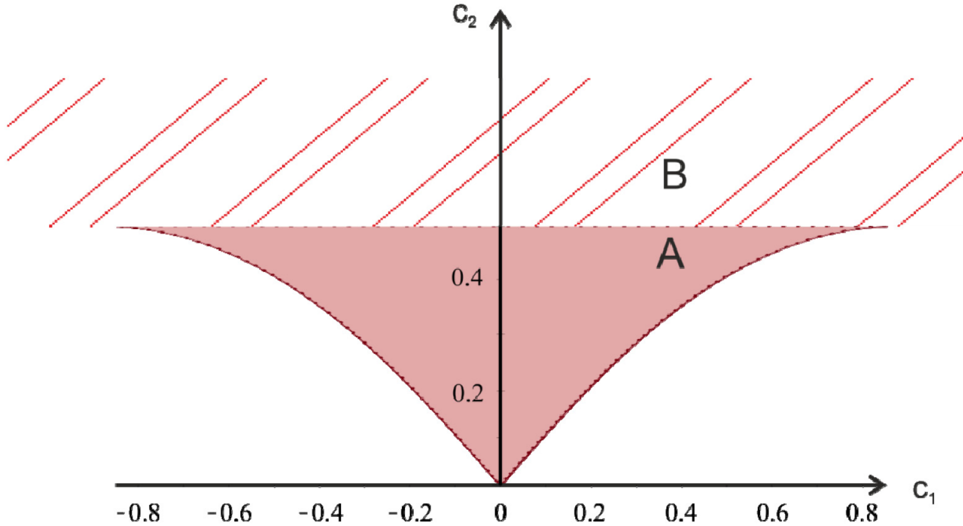

Fig. 2. The allowed regions designed by A and B for the three pole case with a guided mode located at $|k_3| = 1\mu m^{-1}$ derived by previous authors [12,13].

In order to generalize this procedure to higher numbers of poles, we adopt a different approach by using Sturm's Theorem [26] from which we are able to determine whether the conservation-of-energy condition is satisfied or not (see Appendix A for details). The conjugate symmetric leaky poles k_1, k_2 maybe placed anywhere in Region A or Region B but must not be placed at the origin as this would result in the trivial reflection coefficient $r(k) = 0$. The study of the dispersive properties of the designed waveguides was restricted in a region defined by $c_1 = 0.1$, $c_2 = 0.1$ as the inner limit and $c_1 = 4$, $c_2 = 4$ as the outer limit. In all subsequent calculations we assume cladding RI $n_2 = 1.444$, operating wavelength $\lambda = 1.55\mu m$ and guided mode pole $|k_3| = 1\mu m^{-1}$.

Figure 3(a) shows two representative waveguide RI distributions, obtained by inverse scattering the three-pole reflection coefficient with ($c_1 = 0.1$, $c_2 = 0.1$ – design#1) and ($c_1 = 0.85$, $c_2 = 0.4999$ – design#2), using the semi-analytical technique of Pechenick [23]. Design#2 is also compared with the one derived by Lakshmanasamy and Jordan previously using an analytical technique [12], showing an excellent agreement. Figure 3(b) shows the variation of the effective index ($n_{\mathrm{eff}} = \beta/k_0$) as function of $k_0 = 2\pi/\lambda$ for guided modes TE_0 and TE_1, for the two designs. It must be noted that for each design the TE_0 mode effective index at the design wavelength $\lambda = 1.55\mu m$ ($k_0 = 4.05\ \mu m^{-1}$) is $n_{\mathrm{eff}} = 1.4649$, as predicted by Eq. (4) with guided mode pole $|k_3| = 1\mu m^{-1}$. It can be seen that designs with small leaky poles (design#1) resemble more closely a simple quasi-parabolic design. On the other hand, designs with larger conjugate symmetric poles (leaky poles), like design#2, result in features loosely resembling a fiber W-type RI profile and is associated with larger dispersion, as evidenced by the larger slopes of the associated n_{eff}-vs-k_0 curve in Fig. 3(b). In addition, design#2 shows single-mode operation over a much wider range of wavelengths.

#223305 - $15.00 USD Received 16 Sep 2014; revised 24 Dec 2014; accepted 18 Jan 2015; published 3 Feb 2015

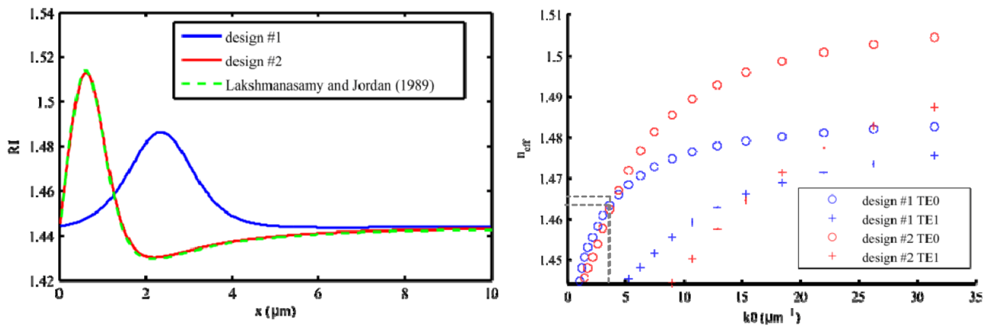

Fig. 3. (a) RI profiles with three-pole rational reflection coefficient designs in region A with $c_1 = 0.1$, $c_2 = 0.1$ (design#1) and $c_1 = 0.85$, $c_2 = 0.499$ (design#2). The exact design#2 obtained by Lakshmanasamy and Jordan [12] (dotted green curve) is also shown for comparison. (b) effective index variation with k_0 for design#1 and #2 (the design point is demarcated by the dashed lines).

So far, in the literature inverse-scattering waveguide designs have been limited to region A [13]. In this work, in order to evaluate the effect of the leaky poles thoroughly, we have studied direct scattered designs, located in both Region A and B, to determine the waveguide dispersion and dispersion slope. The results are summarized in Fig. 4.

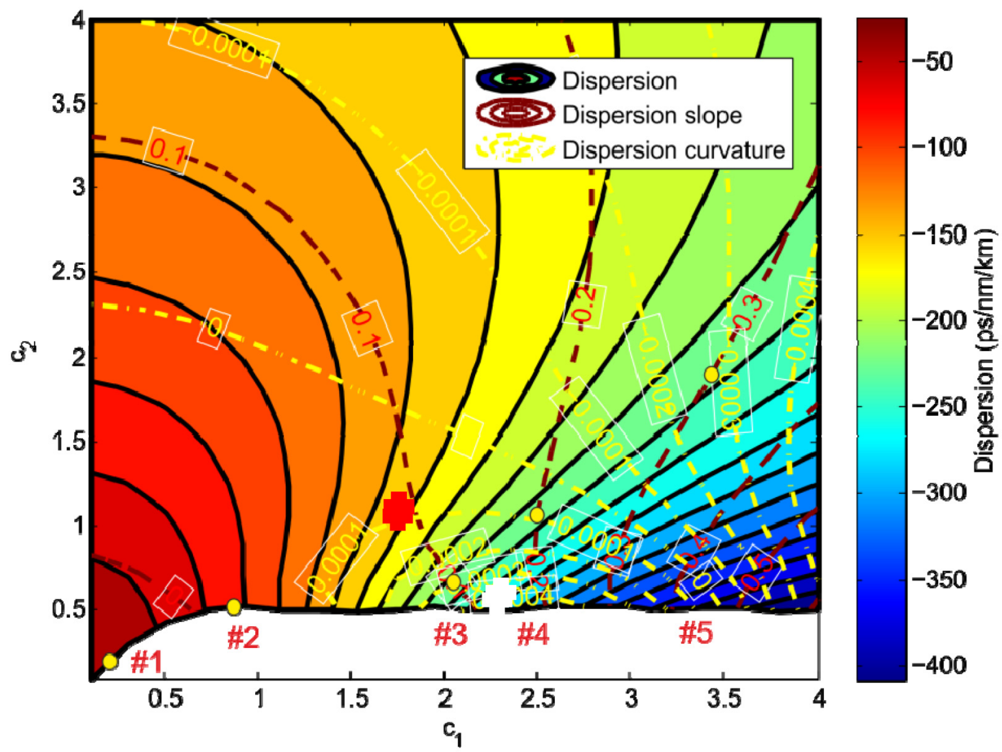

Fig. 4. Waveguide dispersion D_2 (in ps/nm/km), dispersion slope D_3 (in ps/nm^2/km), and dispersion curvature D_4 (in ps/nm^3/km) as a function of leaky pole positions. (designs #1 to #5 are designated by yellow dots).

The second order dispersion coefficient D_2 is defined in terms of the mode effective index $n_{\text{eff}} = \beta/k_0$ as:

#223305 - $15.00 USD Received 16 Sep 2014; revised 24 Dec 2014; accepted 18 Jan 2015; published 3 Feb 2015

$$D_2 = -\frac{\lambda}{c}\frac{d^2 n_{eff}}{d\lambda^2} \tag{12}$$

The higher order dispersion coefficients D_n is given by:

$$D_\text{n} = \text{d}D_{(\text{n}-1)} / \text{d}\lambda, \quad n > 2 \tag{13}$$

D_3 and D_4 are also known as dispersion slope and dispersion curvature expressed in ps/nm^2/km and ps/nm^3/km, respectively. The dispersion map in Fig. 4 can be used to provide the appropriate c_1 and c_2 values for a target D_2, D_3 and D_4 combination.

It can be seen that as previously surmised leakier poles (i.e. larger c_1 and c_2) lead to waveguides with higher waveguide dispersion. In particular, moving out of region A (bottom-left corner of allowed region in Fig. 4) into region B (c_2>0.5) the waveguide dispersion increases from <50ps/nm/km to >400ps/nm/km with more positive dispersion slopes and more negative dispersion curvature. In particular there appears a region close to the edge of the considered region B, on the lower-right hand side, where the largest dispersions are observed.

We also note that designs exist for which the dispersion is constant, and the dispersion slope and dispersion curvature differ. As an example, Fig. 5(a) shows waveguide designs for which D_2 = −215ps/nm/km is constant and D_3 is 0.1ps/nm^2/km (design#3), 0.2ps/nm^2/km (design#4), and 0.3ps/nm^2/km (design#5). The corresponding parameters (c_1,c_2) are (2.0588,0.6541-design#3), (2.5014,1.0885-design#4), and (3.5810,2.1803-design#5). Designs #1 to #5 are designated by yellow dots in Fig. 4.

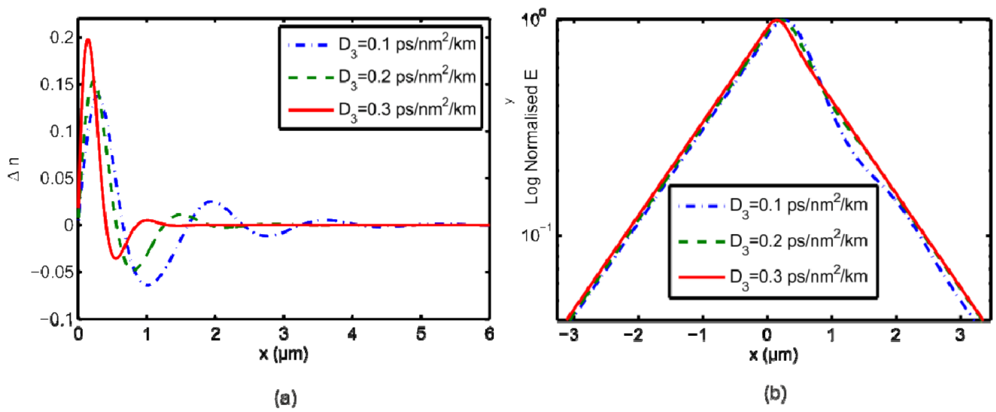

Fig. 5. (a) Waveguide designs and (b) corresponding TE_0 normalized electric field profiles with D_2 = −215ps/nm/km and D_3 = 0.1ps/nm^2/km (design#3), 0.2ps/nm^2/km (design#4) and 0.3ps/nm^2/km (design#5).

We observe from Fig. 5(a) that, for a constant dispersion, increasing the magnitude of the dispersion slope causes the RI profile to narrow and steepen. It is particularly interesting to note that the design with the smallest dispersion slope contains significant trench and ring features, as well as oscillations, which result in substantial dispersion flattening. It should be mentioned that the inversed-scattered profiles can be considered as generalizations of commonly used triple-cladding dispersion compensating fibers. It is well known that for a fixed phase velocity changes in the electric-field/RI overlap are associated with changes in group velocity through the integrals of the scalar approximation method [27]. This is demonstrated in Fig. 5(b) where the electric field of design#3 varies noticeably, when compared with design #5, in accordance with the RI distribution which results in substantial dispersion slope reduction.

#223305 - $15.00 USD Received 16 Sep 2014; revised 24 Dec 2014; accepted 18 Jan 2015; published 3 Feb 2015

In order to further explore the significance of the leaky pole positions on the IS waveguide designs, we have considered separately the effect of their modulus $R = |k_1| = |k_2|$ and their real part magnitude c_1. Figures 6(a) and 6(b) plot the RI modulation profiles for R = 3 and 4, respectively. This demonstrates that while an increase in leaky pole modulus does increase the dispersion, through a narrowing and steepening of the design, it is the increase of parameter c_1 that causes the development of strong RI modulation and larger dispersion.

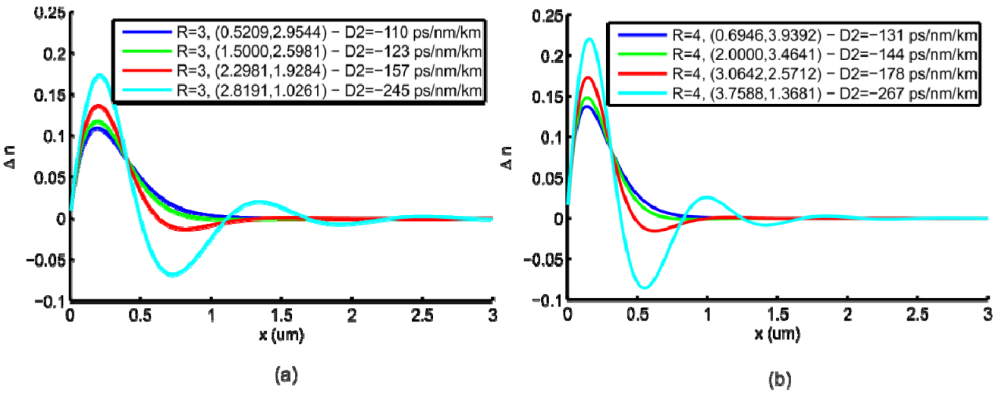

Fig. 6. Effect of leaky pole modulus $R = |k_1| = |k_2|$ on IS waveguide RI modulation. (a) $R = 3$ and (b) $R = 4$.

The dispersion curves of the TE_0 and TE_1 modes for the designs shown in Fig. 6 are plotted in Fig. 7. In addition to higher dispersion, manifested by the increased slope of the dispersion curves at the design wavelength (indicated by dotted lines), the designs with the largest c_1 parameter show wider single mode operation bandwidth (marked by the TE1 cut-off point). Compared with the low dispersion design#1 in Fig. 3, these high dispersion designs show about three time wider single-mode operation bandwidths. This is because of the presence of the RI depression adjacent to the main RI lobe.

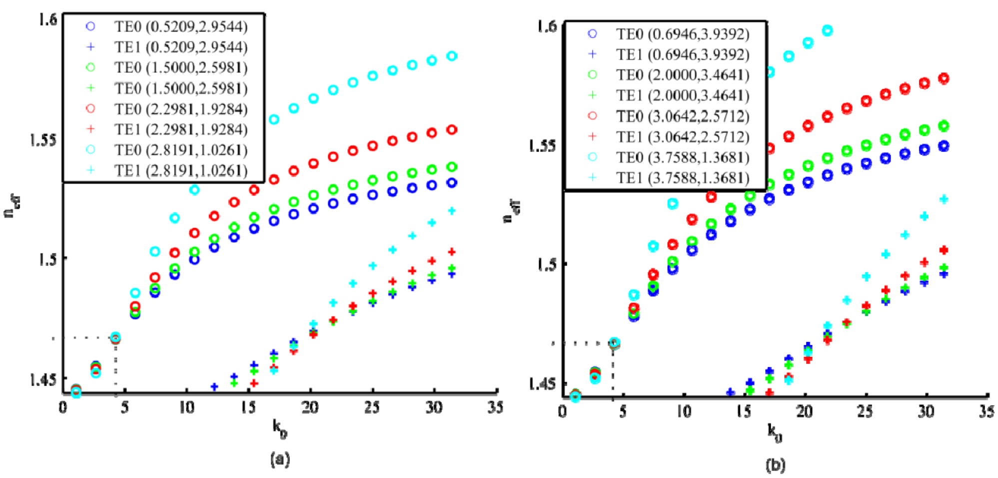

Fig. 7. The dispersion curves (TE_0, TE_1) for (a) R = 3 and (b) R = 4 designs (the design point is demarcated by the dashed lines).

Figure 8(a) shows the effect of c_1 on the waveguide RI profile, for constant c_2. It demonstrates that increasing the c_1 parameter introduces strong RI oscillations with varying period. This also increases the waveguide dispersion as evidenced from the increased slope of the dispersion curves shown in Fig. 8(b).

#223305 - $15.00 USD Received 16 Sep 2014; revised 24 Dec 2014; accepted 18 Jan 2015; published 3 Feb 2015

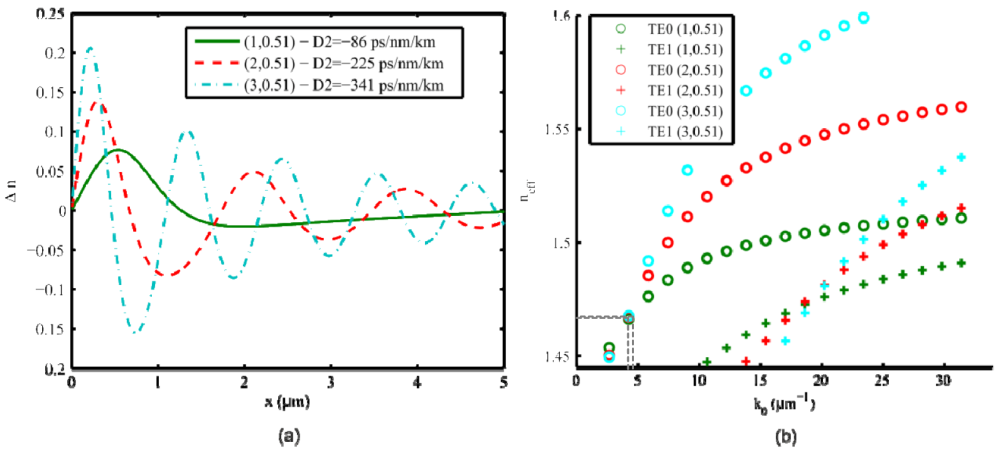

Fig. 8. (a) RI modulation profiles for different c_1 and fixed $c_2 = 0.51$. (b) n_{eff} variation for TE_0 and TE_1 with k_0 (the design point is demarcated by the dashed lines)

In addition to dispersion, RI modulation affects the guided mode field distribution (see Fig. 5(b)), and therefore, the effective mode area. Effective mode area is another important parameter since it defines the strength on waveguide nonlinear effects and the losses between different waveguide structures. The fundamental TE_0 mode effective mode area is calculated by $A_{eff} = (\int|E_y|^2 dA)^2 / \int|E_y|^4\, dA$ and is plotted over the entire (c_1,c_2) parameter space in Fig. 9. It is clearly shown that high dispersion is associated with smaller effective mode areas. The low dispersion designs, located close to the origin within region A, show the largest effective mode areas (of order of 2.8μm^2), while the most dispersive designs, located close to region B lower boundary, show effective mode areas of the order of 1.8μm^2. Such inter-dependence has also been observed in highly dispersive fibers [2,7].

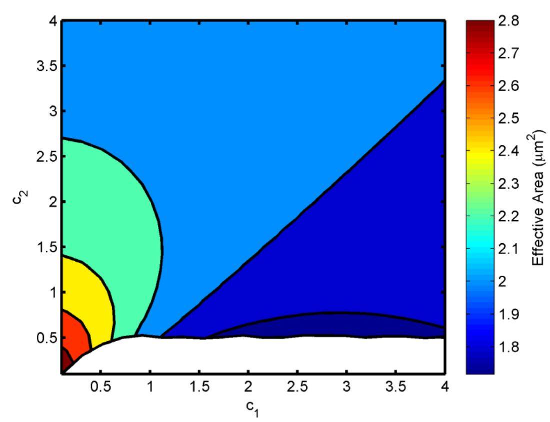

Fig. 9. TE_0 effective mode area over the entire (c_1,c_2) parameter space.

3.2 Five- & Seven-pole reflection coefficients

We have extended the waveguide IS designs to rational reflection coefficients with five poles of the form:

$$r(k) = \frac{k_1 k_2 k_3 k_4 k_5}{(k-k_1)(k-k_2)(k-k_3)(k-k_4)(k-k_5)} \tag{14}$$

with poles k_1, k_2, k_3, k_4, k_5 for which $c_1, c_2, d_1, d_2, a \in R^+$, and

#223305 - $15.00 USD Received 16 Sep 2014; revised 24 Dec 2014; accepted 18 Jan 2015; published 3 Feb 2015

$$k_1 = -c_1 - ic_2, k_2 = c_1 - ic_2; \quad k_3 = -d_1 - id_2, k_4 = d_1 - id_2; \quad k_5 = +ia \qquad (15)$$

It is once again possible to use the semi-analytical IS numerical technique [21] to solve for waveguide designs. This is now a multi-dimensional problem and we only consider specific cases to demonstrate the effect of extra leaky poles.

We first fix two of the leaky poles to $k_{1,2} = \pm 0.85\text{-}i0.4999$ and the guided mode pole to $|k_5| = 1\mu m^{-1}$; as per the leakiest case for three poles in region A considered previously (design#2 in Fig. 3(a) with $D_2 = -72$ps/nm/km, $D_3 = 0.0042$ps/nm^2/km & $D_4 = 0.000049$ ps/nm^3/km). Using Sturm's Theorem we obtain in Fig. 10 the allowable domain and dispersion contours of d_1 and d_2, defining the positions of the other two leaky poles k_3 and k_4. In this case, the allowable domain is totally different to the three-pole case shown in Fig. 4. We notice that in this case the introduction of two extra leaky poles does not change dramatically the waveguide dispersion. Actually, the dispersion for these designs has been limited in magnitude by the size of the initial leaky poles c_1 and c_2 to a value of the order of $D_2 = -72$ps/nm/km.

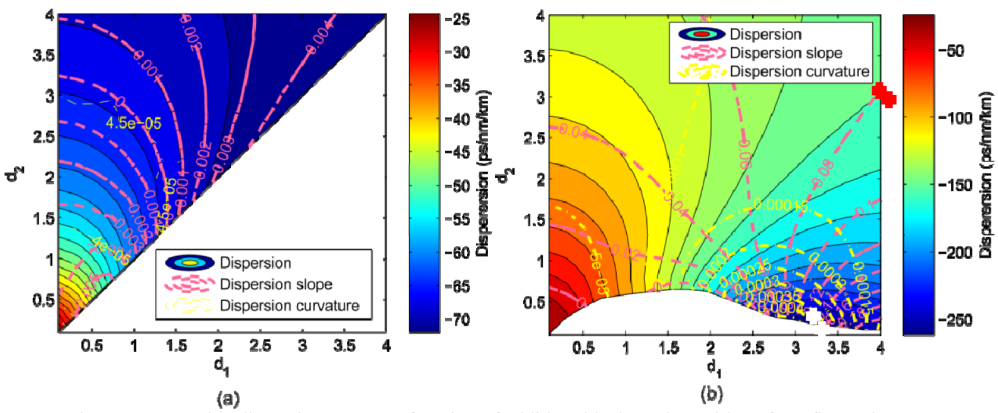

Fig. 10. Waveguide dispersion map as a function of additional leaky pole positions for a five-pole case. (a) $(c_1,c_2)=(0.85,0.4999)$ and (b) $(c_1,c_2)=(1.7,1)$ $|k_5|=1\mu m^{-1}$, $n_2=1.444$ and $\lambda=1.55\mu m$.

Figure 10(b) shows the allowable region and dispersion map with varying d_1, d_2, when the fixed leaky pole position is moved into region B to $(c_1,c_2) = (1.7,1)$. In the three-pole case (see Fig. 4 red cross) this corresponds to $D_2 = -145$ps/nm/km, $D_3 = 0.08$/nm^2/km & $D_4 = 0.00010$/nm^3/km. The allowable (d_1,d_2) region in this case resembles the three-pole one. Once again, though, the obtained waveguide dispersion shows a limited variation around the three-pole values. From the two examples shown in Fig. 10, we deduce that the addition of two extra leaky poles provides very similar results for dispersion tuning as that around the values achieved by the corresponding three-pole case. To demonstrate this, consider a design in Fig. 10 (b) with identical waveguide dispersion and dispersion curvature to that of the three-pole case above, which we also denote by a red cross. We then find that the waveguide dispersion, slope and curvature here are all very similar to those in the existing three-pole case.

To explore this even further, we may choose a three-pole case and a five-pole case indicated by the white crosses in Fig. 4 and Fig. 10(b) respectively, both with waveguide dispersion $D_2 = -261$ps/nm/km and dispersion slope $D_3 = 0.13$ps/nm^2/km but ever so slightly differing dispersion curvature D_4 of 4.41×10^{-4} ps/nm^3/km & 4.29×10^{-4} ps/nm^3/km, respectively. The designs are obtained with $(c_1,c_2) = (2.2775,0.5269)$ and $(c_1,c_2,d_1,d_2) = (1.7,1,3.18,0.22)$, respectively, and the resulting RI distribution is shown in Fig. 11. The two designs show the same qualitative features, and the small difference in D_4 is achieved by

#223305 - $15.00 USD Received 16 Sep 2014; revised 24 Dec 2014; accepted 18 Jan 2015; published 3 Feb 2015

slightly changing the size and periodicity of the RI undulations. These subtle differences are difficult to be captured by traditional iterative solutions, but result naturally by the IS technique.

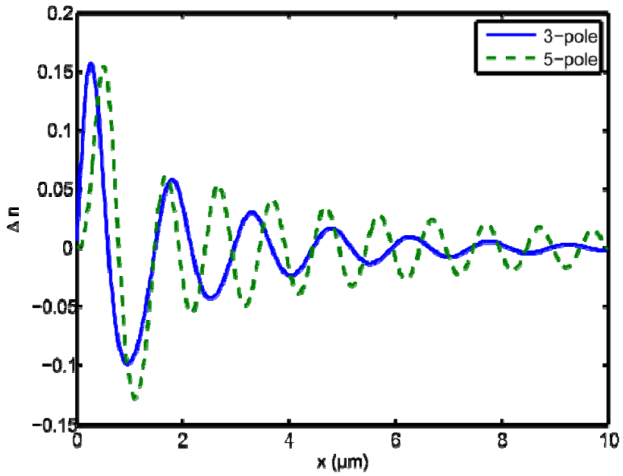

Fig. 11. Three-pole $(c_1,c_2)=(2.2775,0.52692)$ and five-pole $(c_1,c_2,d_1,d_2)=(1.7,1,3.18,0.22)$ designs with identical $D_2=-261\,\text{ps/nm/km}$, $D_3=0.130\,\text{ps/nm}^2\text{/km}$ but differing D_4 ($4.41\text{x}10^{-4}$ ps/nm^3/km & $4.29\text{x}10^{-4}$ ps/nm^3/km). (designs correspond to the 'white crosses' in Fig. 4. and Fig. 10 (b)).

We have also extended even further the waveguide IS designs to rational reflection coefficients with seven poles, by adding two extra leaky poles $k_{5,6} = \pm e_1\text{-}ie_2$. In Fig. 12 we plot the allowable (e_1,e_2) space and resulting dispersion map, using the existing five-pole design point $(c_1,c_2,d_1,d_2) = (1.7,1,3.18,0.22)$, denoted once again by the red cross in Fig. 10(b) and guided pole $k_7 = +i1\mu\text{m}^{-1}$.

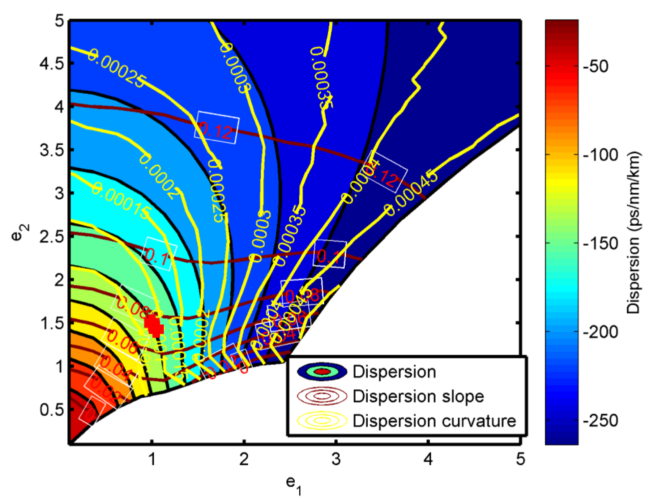

Fig. 12. Seven-pole (e_1,e_2) allowable region and dispersion map, with fixed $(c_1,c_2,d_1,d_2)=(1.7,1,3.18,0.22)$.

We see once again that the design with identical waveguide dispersion and slope to the five-pole design denoted by the red cross has a very similar curvature. It appears that in each case the addition of larger number of poles brings a small but measureable difference in the control of higher order dispersions about a three-pole design corresponding to the leaky pole pair with smallest modulus. This small change is represented by the higher complexity of the refractive index profiles.

4. Summary - Conclusions

In summary we have introduced a semi-analytical IS technique suitable for multipole, rational function reflection coefficients, and used it for the design of dispersion-engineered planar waveguides. The method is exact and stable and compared to other numerical methods it is shown not to introduce roundoff errors and instabilities [23]. Previous works [12,13] have considered a three-pole reflection coefficient with a variable location of two conjugate symmetric leaky poles in the lower half of the k plane in order to obtain a waveguide design with a twofold larger core width than typically obtained by direct scattering techniques. However, the effect and relationship between the leaky pole positions and waveguide dispersion has not been considered to date. In addition, previous authors have not considered the inverse scattering of waveguides for rational reflection coefficients with more than three poles. We have shown that the addition of a larger number of poles, results in different 'pole allowable regions' and through the use of causality arguments in Appendix A we have developed a method to define these allowable regions. The technique is therefore used to derive extensive dispersion maps, including higher dispersion coefficients, corresponding to three-, five- and seven-pole reflection coefficients. The dispersion maps are obtained by varying systematically the pole positions within derived allowable regions. It is shown that common features of dispersion-controlled waveguides such as RI trenches, rings and oscillations come naturally from the IS theory when the magnitude of leaky poles in increased. In particular, while the leaky pole radius does lead to increased core size, trench size and dispersive properties, it is the magnitude of the c_1 parameter near the forbidden region that introduces and controls the period of oscillation in the RI profile. It is also shown that for the three-pole cases, the allowed Region B which has previously not been considered for waveguide designs provides the opportunity for increasingly dispersive designs.

The addition of further poles to the inverse scattering procedure, by which more general and not necessarily rational reflection coefficients can be approximated [13,21], has not been investigated previously and has been shown to offer a small but measureable change in higher order dispersion. It is important to note that the inverse scattering method employed in this work can be applied to an arbitrary number of poles and is therefore not limited. We have also shown that addition of larger number of poles, results in different "pole allowable regions". Using causality arguments, we have developed a method to define these allowable regions.

Although, a very large number of poles is needed to accurately describe general reflections coefficients [21], our work has shown the dispersion response is dominated primarily by the three pole design corresponding to the leaky pole pair with smallest modulus.

We believe that this initial study shows promise for the use of inverse scattering in the design of dispersion-engineered waveguides or fibers and we plan to consider these designs in future work. While we have yet to discover an analytic relationship between pole locations and waveguide dispersion we shall in a future paper present 'engineering curves' relating the phase response of the rational reflection coefficient to the waveguide dispersion.

5. Appendix A

Given a 5-pole reflection coefficient $r(k)$ of the form written in Eq. (14) and using the requirement of conservation of energy $r(k) \leq 1$ for all real k, it is straightforward to derive from $|r(k)|^2 \leq 1$ the requirement that:

$$\frac{A}{B} \leq 1 \tag{16}$$

#223305 - \$15.00 USD Received 16 Sep 2014; revised 24 Dec 2014; accepted 18 Jan 2015; published 3 Feb 2015

Where

$$A \equiv \left(c_1^2 + c_2^2\right)^2 \left(d_1^2 + d_2^2\right)^2 a^2 \tag{17}$$

and

$$B \equiv \left(k^2 + 2kc_1 + c_1^2 + c_2^2\right)\left(k^2 - 2kc_1^2 + c_1^2 + c_2^2\right)\left(k^2 + 2kd_1 + d_1^2 + d_2^2\right) \\ \times\left(k^2 - 2kd_1 + d_1^2 + d_2^2\right)\left(k^2 + a^2\right) \tag{18}$$

We observe that Eq. (16) is true whenever:

$$0 \le B - A \tag{19}$$

If we denote the polynomial in Eq. (19) by $p(k)$ we observe that energy conservation is equivalent to requiring that for all real k :

$$0 \le p(k) \tag{20}$$

Sturm's theorem [26] states that given a polynomial of degree n, $p(k)$ and its derivative $p_1(k)$, there is an associated Sturm chain $S(k) = p(k), p_1(k), \ldots p_n(k)$, where $p_2(k)$ is the remainder of $p(k)$ divided by $p_1(k)$ with reverse sign, and $p_3(k)$ is the remainder of $p_1(k)$ divided by $p_2(k)$ with reverse sign, and so on until a constant is arrived at. Then the number of real roots in the open interval (a,b) is given by:

$$\rho = \nu_a - \nu_b \tag{21}$$

where ν_a and ν_b are the number of sign variations in the Sturm chain $S(a)$ and $S(b)$ respectively. For our case, we require that there are no real roots of $p(k)$ in the interval $(0,\infty)$ and make the necessary substitutions in the above. If we automate the process of determining whether $p(k)$ has real roots in the above interval for any combination of c_1, c_2, d_1, d_2 or as is required through the use of a computer algebra package such as the MAPLE [28] function 'sturm', we obtain the domains illustrated in the contour plots of this paper.

Acknowledgments

We gratefully acknowledge funding support for this work from the Engineering and Physical Sciences Research Council (EPSRC) through the EPSRC Centre for Innovative Manufacturing in Photonics (grant EP/H02607X/1).

#223305 - $15.00 USD Received 16 Sep 2014; revised 24 Dec 2014; accepted 18 Jan 2015; published 3 Feb 2015